

**Strain and ferroelectric soft-mode induced superconductivity in strontium titanate**K. Dunnett,<sup>1</sup> Awadhesh Narayan,<sup>2</sup> N. A. Spaldin,<sup>2</sup> and A. V. Balatsky<sup>1,3,4</sup><sup>1</sup>*Nordita, KTH Royal Institute of Technology and Stockholm University, Roslagstullsbacken 23, SE-106 91 Stockholm, Sweden*<sup>2</sup>*Materials Theory, ETH Zurich, Wolfgang-Pauli-Strasse 27, CH-8093 Zürich, Switzerland*<sup>3</sup>*Institute for Materials Science, Los Alamos National Laboratory, Los Alamos, New Mexico 87545, USA*<sup>4</sup>*Department of Physics, University of Connecticut, Storrs, Connecticut 06269, USA*

(Received 28 December 2017; published 9 April 2018)

We investigate the effects of strain on superconductivity with particular reference to SrTiO<sub>3</sub>. Assuming that a ferroelectric mode that softens under tensile strain is responsible for the coupling, an increase in the critical temperature and range of carrier densities for superconductivity is predicted, while the peak of the superconducting dome shifts towards lower carrier densities. Using a Ginzburg-Landau approach in 2D, we find a linear dependence of the critical temperature on strain: if the couplings between the order parameter and strains in different directions differ while their sum is fixed, different behaviors under uniaxial and biaxial strain can be understood.

DOI: [10.1103/PhysRevB.97.144506](https://doi.org/10.1103/PhysRevB.97.144506)**I. INTRODUCTION**

Strain is one of several mechanisms by which the incipient ferroelectric [1–5] strontium titanate—SrTiO<sub>3</sub> (STO)—can be made ferroelectric [3,6–8]. The interplay between ferroelectricity and superconductivity in STO has been investigated in the context of strontium [9] and oxygen isotope [10,11] substituted STO, finding an increase in the superconducting critical temperature ( $T_c$ ) in samples moved closer to the ferroelectric quantum critical point. Early experimental data showed that compression generally significantly reduces  $T_c$  in STO, with the exception of uniaxial stress at low carrier concentrations where the critical temperature was seen to increase [12]. The possible ferroelectric origin of the superconducting coupling was not considered at the time.

Working within the framework of ferroelectric induced superconductivity in STO [10], we consider the effects of strain on the superconducting dome of STO. Based on this model we predict (1) an increase in  $T_c$  under tensile strain, accompanied by an increase of the range of carrier densities with accessible critical temperatures—i.e., a broadening of the superconducting dome, (2) a shift in the location of the peak of the superconducting dome, and (3) a sharp peak in  $T_c$  signaling the limit of our model which moves to higher carrier concentrations on increasing tensile strain. Although this is at the breakdown point of the model, we still expect this second peak to be present and have observable consequences. Most prominently we find that the effect of strain is substantial, the  $T_c$  more than doubling under experimentally achievable values.

We also find that, under biaxial strain, the different ferroelectric modes behave differently and the changes in  $T_c$  may indicate which ferroelectric mode is most important for superconductivity. Using a simple Ginzburg-Landau model of a uniform superconducting order parameter coupled directly to applied strain, we find a linear dependence of the superconducting critical temperature on strain and go some way towards quantifying the very strong dependence of  $T_c$  on strain in STO compared to elemental superconductors [12,13]. We

find that the increase in  $T_c$  observed in some samples under uniaxial compression [12] can be understood qualitatively if the couplings between the superconducting order parameter and strains in different directions have different strengths.

**II. SUPERCONDUCTING DOME UNDER STRAIN**

One of the key features of superconductivity in STO is the presence of a superconducting dome where  $T_c$  varies with carrier density  $n$  with a maximum at “optimum” doping [14,15]. The generic functional dependence of the critical temperature on strain,  $u = (a - a_0)/a_0$  for lattice constant  $a$  and unstrained value  $a_0$ , and carrier concentration  $n$  can be written as  $T_c = T_0 f(n(u), u)$  where  $T_0$  is the overall scale and  $f$  a dimensionless function assumed to be bounded from above at unity. Since the carrier density  $n$  will be affected by changes in the volume of the unit cell,  $n = n(u)$ . We expect that  $\partial_u T_c / T_0 = f'(n(u), u) = \partial_n f \partial_u n + \partial_u f$ , but the changes in  $n$  due to changes in the volume of the unit cell are small at small strains so  $\partial_u n \approx 0$  (see Appendix A).

To be specific, we use the model of Ref. [10] (also Appendix B) where ferroelectric phonons are assumed to be responsible for the superconducting pairing. This model provides a good description of the superconducting dome within a strong-coupling framework [10] despite the fact that STO is not within the Migdal limit [16]. In the Eliashberg strong-coupling formalism, the BCS coupling constant is [10,17]

$$\lambda = \int_0^\infty d\omega_q \frac{\alpha^2(\omega_q)}{\omega_q} F(\omega_q), \quad (1)$$

where  $\omega_q$  is any phonon dispersion and  $\alpha(\omega_q)$  is the electron-phonon coupling. The main features of soft-mode superconductivity are captured by considering a Van Hove singularity at  $q = 0$ , for which  $F(\omega_q) \sim \delta(\omega_q - \omega_0)$  so  $\lambda \rightarrow \lambda_0 = \alpha^2/\omega_0$ . The critical temperature is then [10,18]

$$T_c = \epsilon_s e^{-\omega_0/\alpha^2} \quad (2)$$

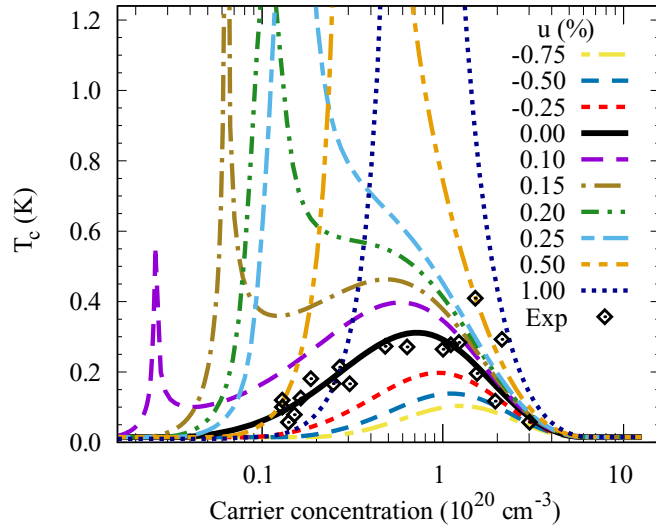


FIG. 1. Superconducting domes for several values of isotropic strain ( $-0.75\% \leq u \leq 1.00\%$ ) in 3D using the model of Ref. [10] and the strain dependence of the ferroelectric mode frequencies from density functional theory (DFT) calculations. The dome broadens and  $T_c$  increases under dilation, with the appearance of a peak at low carrier concentrations that is a signature of  $\omega_q(u) = 0$  in Eq. (1). The scale of maximum  $T_c$  is set by  $T_0 = 7$  K used here. Experimental data from Ref. [14].

where  $\epsilon_s$  sets the energy scale. With constant electron-phonon coupling, this means that  $\omega_0 \rightarrow \omega_0(u)$ . Differentiating Eq. (2) with respect to strain gives

$$\frac{\partial_u T_c(u)}{T_c(u)} = -\frac{\partial_u \omega_0(u)}{\alpha^2}. \quad (3)$$

Experiments on compressed bulk STO found a linear dependence of  $\omega^2$  on applied pressure for both the structural and ferroelectric phonon modes [3,19]. We therefore consider soft modes at  $q = 0$  with a general form under applied strain:  $\omega_0^2(u) = \omega_0^2(0) + bu$  [3]. Calculating  $\partial_u \omega_0(u)$  gives

$$\frac{\partial_u T_c(u)}{T_c(u)} = \frac{-b}{\alpha^2 \omega_0(u)}. \quad (4)$$

The immediate consequence is a sharp rise in the derivative of  $T_c$  with respect to  $u$  near criticality where  $\omega_0 \rightarrow 0$ . The divergence in the derivative is a consequence of the simple model we use and is not physical, yet the peak in  $T_c$  as a result of the quantum critical point is physical and its signature should be observable experimentally.

In Fig. 1, superconducting domes, constructed using the model of Ref. [10], and including the dependence of both the phonon spectra and Fermi energy on strain (details in Appendix B), are plotted for several values of isotropic strain in 3D. The key features of Fig. 1 are a strong increase in the critical temperature under tensile strains, accompanied by a shift of the maximum  $T_c$  towards lower carrier densities, a broadening of the superconducting dome, and the appearance of a sharp secondary peak in  $T_c(n)$  at low carrier concentrations, the value of which is limited by the range of temperatures considered and the tuning over the carrier density. We note that the effect of tensile strain is substantial, with the enhancement in  $T_c$  by more than a factor of two, under experimentally achievable

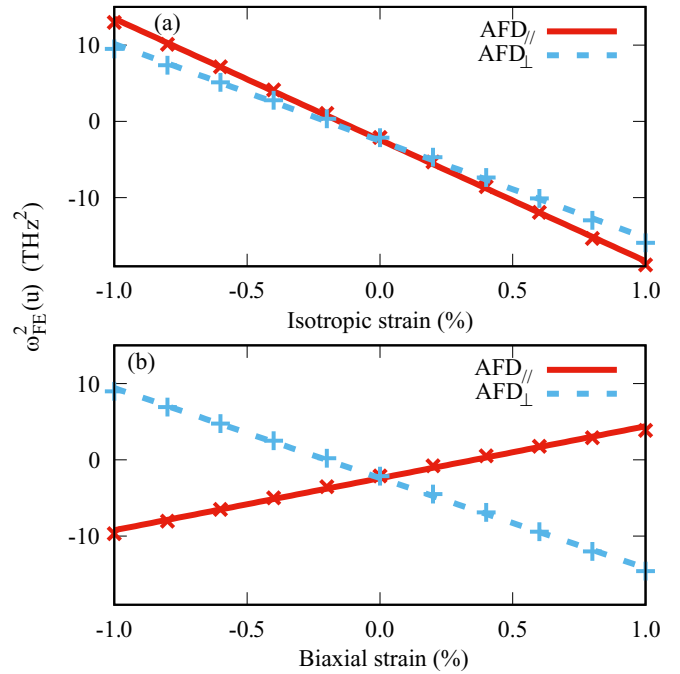


FIG. 2. Squared frequencies of the ferroelectric modes with strain calculated using DFT (details in Appendix C) and their linear fits with slope  $b$ . (a) Isotropic strain:  $b = -15.9, -12.7$  for modes parallel (red, solid) and perpendicular (blue, dashed) to the antiferrodistortive (AFD) axis. Hardening of both modes under compression and softening under dilation characterizes “asymmetric” behavior. (b) Biaxial strain in the basal plane of the tetragonal unit cell:  $b = 6.8, -11.8$ , respectively. One mode softens while the other hardens under both compression and dilation allowing “symmetric” behavior of  $T_c$  whereby it increases or decreases for all strains. The crosses indicate the DFT data points.

strain conditions. Under compression, the dome is narrowed and the critical temperature decreases.

The strong peak in  $T_c$  at low carrier densities is the direct result of the softening of the ferroelectric modes explicitly present in the coupling [Eq. (1)] and its location corresponds exactly to the carrier densities where  $\omega_0(u) = 0$ . Its presence in the case of oxygen isotope substitution [10] was not observed because, in that model, it occurs at much lower carrier densities. Away from these soft-mode induced peaks, the maximum  $T_c$  varies linearly with strain, and a strong deviation, including, as seen at lower carrier concentrations, the possibility for the largest  $T_c$  to occur at intermediate strains, would indicate a soft mode in the coupling mechanism. The strong dependence of the ferroelectric modes in STO on strain potentially allows access to interesting new features by bringing them within the range of carrier concentrations relevant for superconductivity, although the strong, relatively narrow peaks observed here are direct consequences of the model used and appear as kinks in  $T_c$  in a more detailed description that accounts for the anisotropy in the ferroelectric phase [20].

The value of  $b = -13$  (strain as a percentage) used is representative of the linear fits to the squared phonon frequencies in Fig. 2. A smaller value of  $|b|$  would result in weaker changes in  $T_c$  and the peak in  $T_c$  occurring at lower carrier densities for a given strain. A positive value of  $b$  would lead to an

increase in  $T_c$  and the divergence moving towards higher carrier concentrations under compression rather than dilation as seen here.

We can characterize two types of general response: an “asymmetric” response that occurs when the relevant ferroelectric mode softens (frequency decreases) under one sign of strain and hardens for the other so the change in  $T_c$  under tensile (compressive) strain is an extension of the behavior under compressive (tensile) strain. A “symmetric” response is characterized by the variation in  $T_c$  having the same sign for all strains although the gradients may not necessarily be the same on each side of  $u = 0$ .

As seen from the squared frequencies of the ferroelectric modes plotted in Fig. 2, all individual modes give asymmetric behavior under isotropic strain; symmetric behavior is possible in the case of biaxial strain if the critical temperature is controlled by the *softest* rather than a particular mode. Therefore such symmetric or asymmetric behavior under different types of strain could indicate whether the critical temperature is determined by the softest (lowest frequency) ferroelectric mode, or linked to a specific mode or orientation of the tetragonal  $c$  axis, providing an important insight into the superconducting coupling mechanism of STO.

Having examined the effects of isotropic strain on the superconducting dome assuming a ferroelectric soft-mode character for the superconducting coupling, we now develop a simple Ginzburg-Landau model of the strained superconducting system to capture the dominant features of the change in the critical temperature. We focus on the asymmetric response and assume that the coupling strength is independent of strain.

### III. GINZBURG-LANDAU DESCRIPTION

The (Helmholtz) free energy has three parts: the unstrained superconductor in the absence of an applied magnetic field with coefficients  $\alpha = a(T - T_c^0)$  and  $\beta$  [21]; Hooke’s law with strain  $u$  and elastic constants  $\zeta$  [3,6,22]; a part describing the direct coupling between strain and the order parameter  $\psi$  with coupling strengths  $\gamma$  [23,24]:

$$F = \alpha|\psi|^2 + \frac{\beta}{2}|\psi|^4 + \frac{\zeta_{11}}{2}u_1^2 + \frac{\zeta_{22}}{2}u_2^2 + \zeta_{12}u_1u_2 + (\gamma_1u_1 + \gamma_2u_2)|\psi|^2. \quad (5)$$

In order to focus on the qualitative behaviors that may occur, we restrict our analysis to a single uniform superconducting order parameter  $\psi$  in two dimensions with strains applied along the principal axes of a rectangular lattice. The strains  $u_1$  and  $u_2$  therefore denote fractional changes in length along any two of the  $\langle 100 \rangle$  directions of the tetragonal unit cell [6]. Our strain notation is such that, from the general  $\gamma_{\alpha\beta}u_{\alpha\beta}$  coupling between the strain and order parameter permitted [25–27], all shear strains ( $\alpha \neq \beta$ ) are zero and the remaining indices have been contracted. These restrictions are discussed further in Appendix D. All shear strains are assumed to be zero and the volume-preserving reaction along the remaining  $\langle 100 \rangle$  direction is neglected.

Minimizing Eq. (5) with respect to  $\psi^*$  gives a linear change in the critical temperature with applied strain:

$$\Delta T_c = T_c^s - T_c^0 = -u_1\Gamma_1 - u_2\Gamma_2, \quad (6)$$

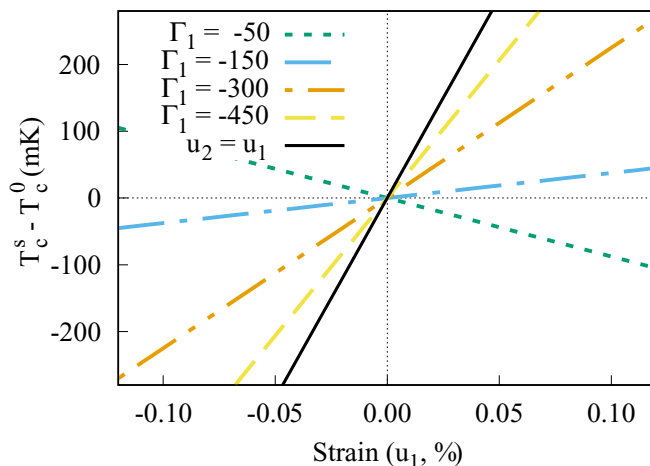


FIG. 3. Change in  $T_c$  as a result of uniaxial applied strain  $u_1$  with  $u_2 = -\nu u_1$ . Varying (negative)  $\Gamma_1$  while keeping  $\Gamma_1 + \Gamma_2 = -600$  K leads to both an increase and a decrease of  $T_c$  under uniaxial compression depending on the exact value of  $\Gamma_1$ .

where scaled coupling constants,  $\Gamma = \gamma/a$ , with units of temperature (K) have been introduced. In the case of symmetry-preserving strain,  $u_1 = u_2 = u$ , and we define  $\Gamma = \Gamma_1 + \Gamma_2$  so Eq. (6) simplifies to

$$\Delta T_c^{lm} = -\Gamma u. \quad (7)$$

There is a simple linear dependence of  $T_c$  on strain and the behavior would reflect an asymmetric nature of the ferroelectric modes under strain. Detail of how an estimate for  $\Gamma$  can be extracted from experimental pressure data is contained in Appendix E.

Meanwhile, when the only applied strain is  $u_1$ , the relaxation of the lattice determines  $u_2$  so  $u_2 = -\nu u_1$  where  $\nu$  is Poisson’s ratio [28] ( $\nu \approx 0.25$  for bulk STO [29]), and the couplings to strains in the different directions become important. For simplicity, we neglect the effects of the change of the crystal symmetry and assume that, at least for small strains, the dominant irreducible representation of the order parameter will be the same as the unstrained system, although in principle they will differ [30]. The change in the critical temperature is again linear in the applied (uniaxial) strain:

$$\Delta T_c^{ux} = -u_1(\Gamma_1 - \nu\Gamma_2). \quad (8)$$

Assuming that  $\Gamma_1$  and  $\Gamma_2$  have the same sign, the relative sizes of  $\Gamma_1$  and  $\Gamma_2$  will determine the sign of  $\Delta T_c^{ux}$ , with no change in  $T_c$  due to uniaxial strain if  $\Gamma_1 = \nu\Gamma_2$ . In Fig. 3, the value of  $\Gamma = \Gamma_1 + \Gamma_2$  is fixed at  $\Gamma = -600$  K as determined from hydrostatic pressure data [12,19] and  $\Delta T_c^{ux}$  for different choices of  $\Gamma_1$  are plotted showing that both decreases and increases in  $T_c$  under uniaxial compressive strains are possible. As discussed in Appendix D, for strains applied to an initially square lattice,  $\Gamma_1 = \Gamma_2$ . However, if the initial 2D lattice is rectangular,  $\Gamma_1 \neq \Gamma_2$  is permissible and, for  $\Gamma_1$  sufficiently small, an increase of  $T_c$  under compression may occur.

In experiments, linear  $\Delta T_c$  under uniaxial compression in the  $[100]$  direction has been observed to be either positive or negative depending on the carrier concentration, while in all other cases, compression led to a decrease in  $T_c$  that

was strongest for hydrostatic pressure [12]. The analysis presented here indicates that at different points across the superconducting dome the relative sizes of  $\Gamma_1$  and  $\Gamma_2$  may differ while their sum is (approximately) constant across the superconducting dome [12,19]. Since the observed increase in  $T_c$  under uniaxial compression is weak compared with the decrease under hydrostatic pressure [12], the possibility of  $\Gamma_1 > 0$  has not been considered.

Further, the linear changes of  $T_c$  under various stress configurations have been observed over a broad range ( $-0.12 \lesssim \Delta T_c \lesssim 0.031$  K) of temperatures for  $T_c^0 = 0.27$  K [12], so, although the limit of a Landau analysis is usually  $(T - T_c^0)/T_c^0 \ll 1$ , the linear variation of  $T_c$  considered here is likely to be representative of strains giving a broad range of  $T_c/T_c^0$ . Moreover, changes in  $T_c$  larger than 10% for lattice changes of  $\sim 0.1\%$  have also been observed in two dimensionally doped STO where the size of the effect was attributed to the variation of dielectric properties with the orientation of tetragonal domains [31].

In the above discussion, we considered a 2D superconducting order parameter and the results presented are qualitative in nature. The example with  $u_1 = u_2$  reflects 3D isotropic strain while the uniaxial case ( $u_2 = -\nu u_1$ ) is representative of all strain configurations where the lattice relaxes in directions perpendicular to the applied strain but otherwise preserves the pseudocubic structure of the unit cell. The value of  $\Gamma$  is overestimated, but the behaviors are representative of those that may occur.

The interplay between ferroelectricity and superconductivity in STO has been examined for both oxygen isotope substitution [10] and a combination of oxygen depletion and calcium doping [9], with critical carrier densities  $10^{19} < 10^{20}$  cm $^{-3}$  beyond which the ferroelectric-like order is destroyed [9,10]. Both bulk [3] and thin-film STO [6,8] samples become ferroelectric beyond critical strains on the range of 0.3% [6,8,32–34]. Assuming that the critical carrier density that destroys ferroelectric order in STO does not depend strongly on the origin of the ferroelectric order, we expect ferroelectric order and superconductivity to occur within the same range of carrier densities for strained systems. The proposed strain tunability of STO superconductivity builds on these ideas and provides an alternative test of the role of ferroelectric criticality in STO superconductivity with several distinct signatures. While the discussion has focused on bulk STO, we expect similar effects to occur in interfacial superconductivity of STO-based systems.

#### IV. CONCLUSIONS

In conclusion, we have considered the effects of strain on superconductivity in STO in two situations. First, we assumed that the superconducting coupling is caused by the ferroelectric modes that are present due to the incipient ferroelectric nature of STO. This led to an increase of  $T_c$  under isotropic tensile strain, a broadening of the superconducting dome, and a shift of the maximum  $T_c$  towards lower carrier densities. We found that strain is an efficient way to control the soft-mode induced superconductivity, with the  $T_c$  more than doubling under small strains. The behaviors are exactly opposite under compression. We note that differences between isotropic and biaxial strain

experiments may provide insight into the relative importance of the ferroelectric modes parallel and perpendicular to the tetragonal  $c$  axis for the superconducting pairing. Although reference has been made to STO, the behaviors observed are expected to be general for any superconductor where pairing is mediated by softening ferroelectric modes, such as in KTaO $_3$  [35]. One important feature of strained STO is that small tensile strains are sufficient to bring the ferroelectric quantum critical point, characterized by  $\omega_0(u) = 0$ , to carrier densities that are well within the superconducting dome, leading to a distinct signature in  $T_c$  [20]. Thus strain tuning is expected to be a versatile means of investigating the interplay between superconductivity and ferroelectricity in STO.

In order to understand experimental data of linear changes of  $T_c$  under various strain configurations, we also considered a simple Ginzburg-Landau analysis of a uniform 2D superconductor under strain in which there is a linear dependence—very strong for STO—of  $T_c$  on strain. The observed qualitative differences between uniaxial and isotropic strain (hydrostatic pressure) [12] can be understood by considering that the couplings to strain in different directions may depend on carrier density while their sum remains fixed.

#### ACKNOWLEDGMENTS

We are grateful for enlightening discussions with R. M. Geilhufe, C. Triola, and Y. Kedem. The work was supported by the US DOE BES E3B7, by VILLUM FONDEN via the Centre of Excellence for Dirac Materials (Grant No. 11744) and the Knut and Alice Wallenberg Foundation, and the European Research Council under the European Union’s Seventh Framework Program (FP/2207-2013)/ERC Grant Agreement No. DM-321031. A.N. and N.A.S. acknowledge support from ETH-Zurich. Calculations were performed at ETH-Zurich (Euler cluster) and at the Swiss National Supercomputing Centre (Project ID p504).

#### APPENDIX A: ON ASSUMING $n(u) \approx n(0)$

The carrier density is defined as the number of free electrons  $n_e$  per unit cell of volume  $V$ . In the unstrained tetragonal unit cell,  $V = V_0 = a_0^2 c$ . If strain is applied uniaxially along one  $\langle 100 \rangle$  axis and the lattice is allowed to relax in the two perpendicular directions, the Poisson’s ratios for the relaxation are needed. Since STO has a tetragonal unit cell, the Poisson’s ratios in the in-plane  $v_a$  and  $c$ -axis  $v_c$  directions are, in principle, different.

The volume of the strained unit cell is  $V(u) = (a_0 + \delta a_{[100]})(a_0 + \delta a_{[010]})(c + \delta c_{[001]})$  for changes  $\delta a, \delta c$  in the lattice constants. With strain defined as the fractional change in the lattice constants, i.e.,  $u = (a - a_0)/a_0$ , the strains resulting from the controlled deformation in the  $[100]$  direction are  $u_{[010]} = \delta a_{[010]}/a_0 = -v_a u_{[100]}$  and  $u_{[001]} = \delta c_{[001]}/c_0 = -v_c u_{[100]}$ . Thus,  $V(u) = V_0(1 + u_{[100]})(1 - v_a u_{[100]})(1 - v_c u_{[100]})$ .

Considering the case of a small strain applied in the  $[100]$  direction, only the linear term is kept in expanding  $V(u) \approx V_0[1 + u_{[100]}(1 - v_a - v_c)]$ , from which

$$n(u) \approx n_0[1 + u_{[100]}(1 - v_a - v_c)]. \quad (\text{A1})$$

For many materials  $\nu \sim 0.3$  [28] and for cubic STO  $\nu \approx 0.25$  [29]. Further, the absolute maximum of  $\nu$  is 0.5 [28] so tetragonal STO probably has  $\nu_a \neq \nu_c \sim 0.25$ , implying that the limit of carrier density under uniaxial strain is

$$n(u) \approx n_0(1 + 0.5u_{[100]}).$$

If strain is applied equally to more than one axis, then the effective  $\nu$  of the second axis is  $-1$ ; ignoring or forbidding relaxation of the third axis is equivalent to  $\nu = 0$  for this axis. Isotropic strain ( $u_{[100]} = u_{[010]} = u_{[001]}$ ) that preserves the tetragonal unit cell has the maximum change in volume, with the resulting change in carrier density:

$$n(u) \approx n_0(1 - 3u).$$

Thus, at least for small strains (1% strain corresponds to  $u = 0.01$ ), the change in carrier density due to strain is small and can be neglected.

### APPENDIX B: DESCRIPTION OF SUPERCONDUCTING DOME

The superconducting dome is constructed by combining Eliashberg strong-coupling theory with the standard expression for the superconducting critical temperature [10,17]. The coupling is given by Eq. (1) of the main text [10]:

$$\lambda = \int_0^\infty d\omega \frac{\alpha^2(\omega)}{\omega} F(\omega)$$

with  $\omega = \omega_q$ . The frequencies of the soft ferroelectric mode excitations around the paraelectric ground state are given by

$$\omega_q^2(u) = 4\Gamma_f[\Gamma_f - 2J \cos(q)] + bu, \quad (\text{B1})$$

in which  $\Gamma_f = A + BE_f^2 + CE_f$  with  $E_f$  weakly dependent on strain through the carrier density  $n(u) = n_0/([1 + u]^3) \approx n_0(1 - 3u)$ . If  $b > 0$ ,  $\omega_q^2$  decreases with compressive strain, while it would increase under compression for  $b < 0$ . On the basis of our DFT calculations and existing experimental data [3,12,19], we believe that the latter scenario is realized in isotropically strained STO. For isotropic strain, the coupling is

$$\lambda \sim \int_{-\pi}^{\pi} \frac{dq}{\sqrt{4\Gamma_f[\Gamma_f - 2J \cos(q)] + bu}}. \quad (\text{B2})$$

The ratio  $\Gamma_f/2J$  is unity on the ferroelectric quantum critical line so  $2J = 1$  is used for simplicity. The values of the parameters chosen are such that  $\Gamma_f = 1$  at zero doping and strain:  $A = 1.14$ ,  $B = 10^{-6} \text{ K}^{-2}$ , and  $C = 2.5 \times 10^{-3} \text{ K}^{-1}$ . The Fermi energy,  $E_f$ , is converted to carrier concentration in order to plot the superconducting dome [10].

The standard expression for the critical temperature is [10,17]

$$1 = \frac{\lambda}{2\pi^2} \int_{-E_f}^0 d\epsilon N(\epsilon) \frac{\tanh(\epsilon/2T_c)}{\epsilon},$$

where  $\epsilon$  is the energy relative to the Fermi energy  $E_f$  and  $N(\epsilon)$  is the density of states. The two limits are set by  $N(\epsilon) = 0$  for  $\epsilon \leq -E_f$  and  $\epsilon = 0$  at  $E_f$ . For low doping, the relevant energy range is near  $-E_f$  and the density of states in 3D is  $N(\epsilon) \sim \sqrt{\epsilon + E_f}$ . A change of variables  $x = \epsilon/T_c$  is made

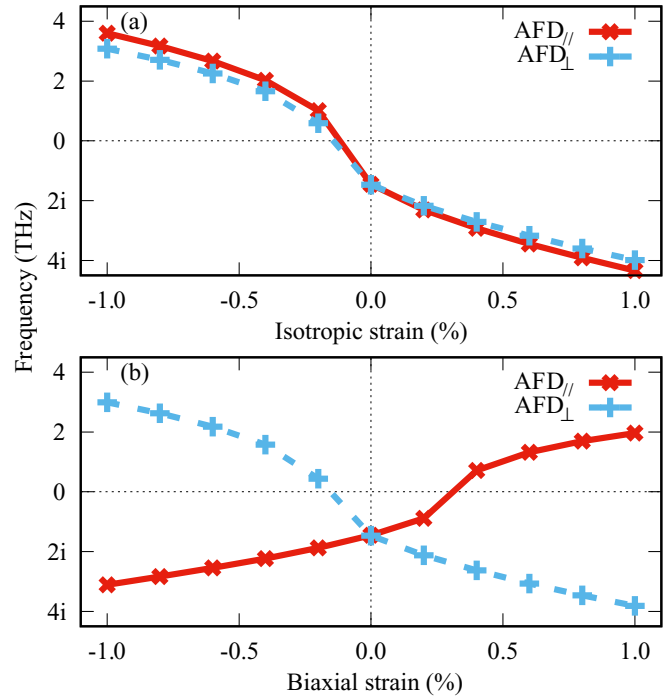


FIG. 4. Variation of the ferroelectric mode frequencies with (a) isotropic strain and (b) biaxial strain in the basal plane of the tetragonal unit cell. The solid blue curves are for the mode perpendicular to the axis of the antiferrodistortive (AFD) rotations and the dashed red curves correspond to the mode parallel to the AFD axis; in both cases, the crosses mark the DFT data points. The imaginary frequencies correspond to unstable phonon modes.

and we have to solve [10,17]

$$\frac{D}{\lambda} = \sqrt{T_c} \int_{-E_f/T_c}^0 dx \sqrt{x + E_f/T_c} \frac{\tanh(x/2)}{x} \quad (\text{B3})$$

numerically with  $D = 190 \text{ K}^{1/2}$  and  $\lambda$  given by Eq. (B2).

### APPENDIX C: FERROELECTRIC MODE IN STRAINED STO

To gain an insight into the behavior of ferroelectric modes under strain and carrier doping, we carried out first-principles calculations. Density functional calculations were performed using the Vienna *Ab initio* Simulation Package (VASP) [36], with the PBEsol approximation to the exchange correlation functional [37]. We used the default projector augmented wave pseudopotentials, and the wave function was expanded in plane waves up to a cutoff of 550 eV. The Brillouin zone was sampled using an  $8 \times 8 \times 6$   $k$ -point grid. We used the low-temperature tetragonal structure of SrTiO<sub>3</sub> and relaxed the structures until the forces were less than  $10^{-4} \text{ eV/\AA}$ . The phonon calculations were performed using the PHONOPY code [38], employing 80-atom supercells and a  $4 \times 4 \times 6$   $k$ -point mesh.

We considered two scenarios: uniform change in lattice constants (isotropic strain corresponding to hydrostatic pressure conditions) and biaxial strain in the basal plane of the tetragonal unit cell. Our results for the frequencies of the ferroelectric (FE) mode are shown in Fig. 4. A uniform reduction in the lattice constants hardens the FE mode and the frequency becomes positive for  $\sim 0.1\%$  reduction in the lattice constants [Fig. 4(a)].

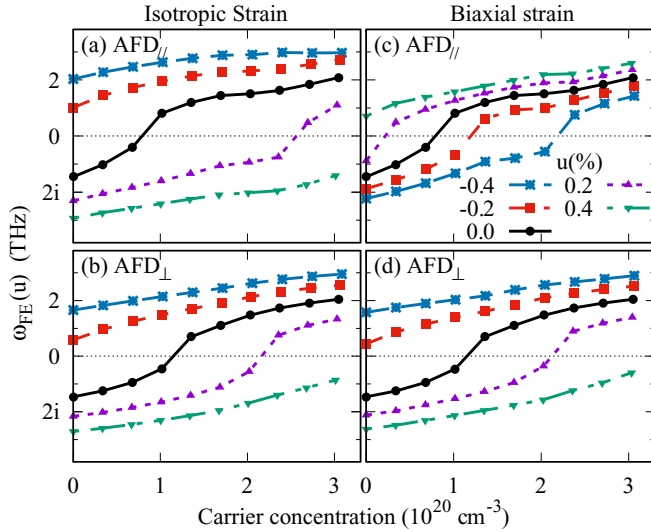


FIG. 5. Ferroelectric mode frequencies at different strain values and across a range of carrier densities. Left [(a), (b)]: Isotropic strain affecting only the volume of the unit cell. Right [(c), (d)]: Biaxial strain in the basal plane of the tetragonal unit cell. Top row [(a), (c)]: FE mode parallel to the AFD (tetragonal  $c$ ) axis. Bottom row [(b), (d)]: FE mode perpendicular to the AFD axis. The imaginary frequencies denote unstable phonon modes.

On the other hand, with an increase in volume (negative hydrostatic pressure), the FE-mode frequencies become more imaginary, indicating a stronger FE instability.

Meanwhile, under biaxial strain, the behavior of FE modes parallel and perpendicular to the axis of antiferrodistortive (AFD) rotations, i.e., the  $c$  axis, is opposite [Fig. 4(b)]. For an in-plane compressive strain the FE modes perpendicular to the AFD axis harden, while the mode parallel to the AFD axis becomes more unstable. Under tensile strain, the situation is reversed: modes perpendicular to the AFD axis soften and the mode parallel to the AFD axis is stabilized. Although different FE modes are softening, the overall behavior is symmetric under strain. Uniaxial strain is expected to mirror the biaxial case analyzed here, although the anisotropy between the two AFD modes may be greater and, in some geometries, the two modes perpendicular to the AFD axis may split.

To understand the effect of carrier doping on the ferroelectricity and its interplay with strain, we carried out density functional calculations by adding electrons to the unit cell (a background compensating charge was added to maintain overall charge neutrality). The results are shown in Fig. 5 for the FE modes parallel and perpendicular to the AFD axis, under both isotropic and biaxial strain. The effect of electron doping is to harden the FE-mode frequency: driving the system closer to the quantum critical point if unstable phonon modes are present and further away from the quantum critical point if all FE modes are initially stable.

#### APPENDIX D: SYMMETRY CONSIDERATIONS FOR COUPLING TERMS

In the free energy, the general coupling term between strain and the superconducting order parameter is [25–27]

$$\tilde{\gamma} \mathbf{u} |\psi|^2,$$

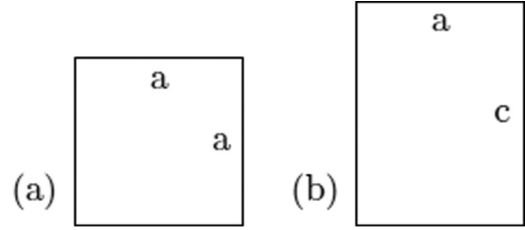


FIG. 6. Sketches of two planes of the unstrained tetragonal unit cell that permit either (a) equal (square basal plane) or (b) different (rectangular  $ac$  plane) coupling strengths between strain and the order parameter along the perpendicular strain directions considered.

where  $\mathbf{u}$  is the symmetric strain tensor with elements  $u_{\alpha\beta}$ ,  $\alpha, \beta \in \{1, 2, 3\} \equiv \{x, y, z\}$  in 3D, or  $\{1, 2\}$  in 2D and  $\tilde{\gamma}$  some coupling.

The free energy transforms as a scalar—the identity; assuming a uniform  $s$ -wave order parameter,  $|\psi|^2$  also transforms as the identity.  $\mathbf{u}$  is a rank-two tensor [28] so  $\tilde{\gamma}$ , which couples a rank-two tensor to a scalar is also a rank-two tensor [39]. Performing the tensor contraction leads to a prefactor of each  $u_{\alpha\beta}$  containing a combination of the various  $\tilde{\gamma}_{\alpha\beta}$  elements.

Considering only strains that preserve the pseudocubic symmetry of the unit cell (i.e.: setting all shear strains, where  $\alpha \neq \beta$ , to zero), and considering the two-dimensional model, the coupling term can therefore be written in a simplified form as

$$\gamma_1 u_1 + \gamma_2 u_2 \quad (\text{D1})$$

where  $\gamma_{1,2}$  contain combinations of the original  $\tilde{\gamma}_{\alpha\beta}$  elements and  $u_{1,2}$  are  $u_{11,22}$ .

A cubic unit with symmetry  $O_h$  has all axes equivalent so  $\gamma_1 = \gamma_2$ . However, in the tetragonal unit cell of low-temperature STO, symmetry  $D_{4h}$ , the two couplings may be different depending on which view is considered. The structural phase transition means that  $\gamma_c \neq \gamma_a$ ; then, for configurations that involve strains along the tetragonal  $c$  axis,  $u_c$ ,  $\gamma_1 \neq \gamma_2$ . Thus, depending on the view of the tetragonal unit cell assumed in the 2D discussion, the couplings to  $u_1$  and  $u_2$  may differ. The two possible initial 2D unit cell symmetries are sketched in Fig. 6.

In the case of isotropic strain where  $u_1 = u_2$ , the coupling strength is the sum  $\gamma_1 + \gamma_2$  and would therefore result in a different slope to the change in  $T_c$ . It is when  $u_2 = -\nu u_1$  that the effect of different  $\gamma$  values (and competing contributions to the change in  $T_c$ ) becomes significant, as demonstrated in Fig. 3 of the main paper.

#### APPENDIX E: COUPLING STRENGTHS FROM PRESSURE (STRESS) DATA

The strain-order parameter coupling strengths must be determined from experimental data which are often in terms of applied pressure. By introducing the Gibbs free energy,  $G = F - \sum_{\lambda} \sigma_{\lambda} u_{\lambda}$ , the stresses (negative pressures)  $\sigma_{\lambda}$  are now present. Assuming isotropic, symmetry-preserving strains from hydrostatic pressure,  $u = u_1 = u_2$ ;

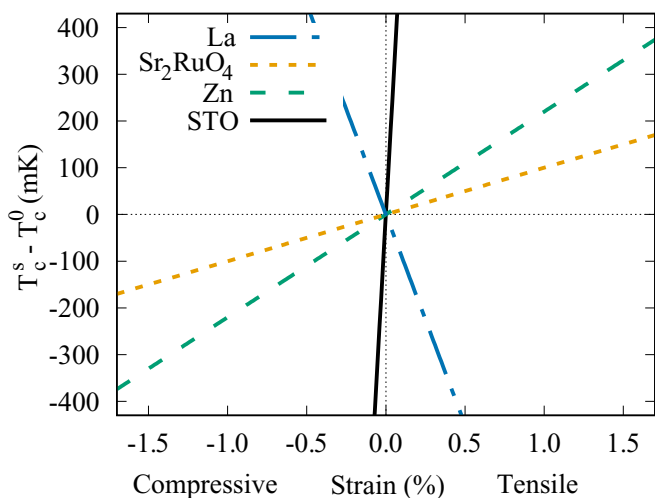


FIG. 7. Linear change in the superconducting critical temperature (asymmetric response continued from experimental behavior under compression [12]) as a result of isotropic strain [Eq. (7) of main text] for several materials and  $|u| < 1.7\%$ . The materials and scaled coupling strengths are STO,  $\Gamma = -600$  K; Zn,  $\Gamma = -20$  K;  $\text{Sr}_2\text{RuO}_4$ ,  $\Gamma = -10$  K; and La,  $\Gamma = 90$  K.

$\sigma_1 = \sigma_2 = \sigma \Rightarrow G = F - 2\sigma u$ , and solving  $\partial G/\partial u = 0$  [3,6,22] gives the equilibrium value of strain:

$$\bar{u} = \frac{\sigma}{\zeta} - \frac{\gamma}{2\zeta} |\psi|^2,$$

which is substituted into the free energy ( $\zeta = \zeta_{11} + \zeta_{12}$ ;  $\gamma = \gamma_1 + \gamma_2$ )

$$G(\sigma) = |\psi|^2 \left( \alpha + \frac{\sigma\gamma}{2\zeta} \right) + \frac{|\psi|^4}{2} \left( \beta - \frac{\gamma^2}{2\zeta} \right) - \frac{\sigma^2}{\zeta}.$$

Minimization with respect to  $\psi^*$  gives

$$\Delta T_c(\sigma) = T_c(\sigma) - T_c^0 = -\frac{\Gamma\sigma}{2\zeta}. \quad (\text{E1})$$

Although superconductivity in STO occurs at temperatures well below the cubic-tetragonal structural phase transition at about 105 K [3,40–43], the elastic constants of STO at low temperatures are not well known [12,44,45] so we use values extrapolated from the high-temperature cubic unit cell:  $\zeta_{11} = \zeta_{22} = 3.36$ ,  $\zeta_{12} = 1.07 \times 10^{11}$  Pa [3,6].

In Fig. 7 the changes in the critical temperature that would occur with coupling constants calculated from hydrostatic pressure data for STO [12,19], zinc and lanthanum [13], and [110] strain data for  $\text{Sr}_2\text{RuO}_4$  [24] (assuming [110]  $\rightarrow u_1 = u_2$ ) are plotted for a range of strains that can be achieved in STO films by lattice mismatch to a substrate [46]. The range of temperatures is chosen to lie near the maximum  $T_c$  observed in unstrained STO [14].

We note that the value of  $\Gamma$  obtained here is certainly overestimated, as might be expected since the analysis considers a 2D system but has used hydrostatic pressure data. However, although the actual coupling strengths are not accurate, a more precise analysis would have a similar effect on all examples and the relative sizes of the  $\Gamma$  values for the different materials are representative.

- [1] J. M. Worlock and P. A. Fleury, *Phys. Rev. Lett.* **19**, 1176 (1967).  
 [2] W. G. Stirling, *J. Phys. C* **5**, 2711 (1972).  
 [3] H. Uwe and T. Sakudo, *Phys. Rev. B* **13**, 271 (1976).  
 [4] K. A. Müller and H. Burkard, *Phys. Rev. B* **19**, 3593 (1979).  
 [5] H. W. Jang, A. Kumar, S. Denev, M. D. Biegalski, P. Maksymovych, C. W. Bark, C. T. Nelson, C. M. Folkman, S. H. Baek, N. Balke, C. M. Brooks, D. A. Tenne, D. G. Schlom, L. Q. Chen, X. Q. Pan, S. V. Kalinin, V. Gopalan, and C. B. Eom, *Phys. Rev. Lett.* **104**, 197601 (2010).  
 [6] N. A. Pertsev, A. K. Tagantsev, and N. Setter, *Phys. Rev. B* **61**, R825 (2000).  
 [7] W. J. Burke and R. J. Pressley, *Solid State Commun.* **9**, 191 (1971).  
 [8] J. H. Haeni, P. Irvin, W. Chang, R. Uecker, P. Reiche, Y. L. Li, S. Choudhury, W. Tian, M. E. Hawley, B. Craigo, A. K. Tagantsev, X. Q. Pan, S. K. Streiffer, L. Q. Chen, S. W. Kirchoefer, J. Levy, and D. G. Schlom, *Nature (London)* **430**, 758 (2004).  
 [9] C. W. Rischau, X. Lin, C. P. Grams, D. Finck, S. Hams, J. Engelmayer, T. Lorenz, Y. Gallais, B. Fauqué, J. Hemberger, and K. Behnia, *Nat. Phys.* **13**, 643 (2017).  
 [10] J. M. Edge, Y. Kedem, U. Aschauer, N. A. Spaldin, and A. V. Balatsky, *Phys. Rev. Lett.* **115**, 247002 (2015).  
 [11] A. Stucky, G. W. Scheerer, Z. Ren, D. Jaccard, J.-M. Poumirol, C. Barreateau, E. Giannini, and D. van der Marel, *Sci. Rep.* **6**, 37582 (2016).  
 [12] E. R. Pfeiffer and J. F. Schooley, *J. Low Temp. Phys.* **2**, 333 (1970).  
 [13] N. B. Brandt and N. I. Ginzburg, *Contemp. Phys.* **10**, 355 (1969).  
 [14] C. S. Koonce, M. L. Cohen, J. F. Schooley, W. R. Hosler, and E. R. Pfeiffer, *Phys. Rev.* **163**, 380 (1967).  
 [15] X. Lin, G. Bridoux, A. Gourgout, G. Seyfarth, S. Krämer, M. Nardone, B. Fauqué, and K. Behnia, *Phys. Rev. Lett.* **112**, 207002 (2014).  
 [16] M. Thiemann, M. H. Beutel, M. Dressel, N. R. Lee-Hone, D. M. Broun, E. Fillis-Tsirakis, H. Boschker, J. Mannhart, and M. Scheffler, *arXiv:1703.04716*.  
 [17] D. van der Marel, J. L. M. van Mechelen, and I. I. Mazin, *Phys. Rev. B* **84**, 205111 (2011).  
 [18] G. D. Mahan, *Many-Particle Physics*, 2nd ed. (Plenum Publishers, New York, 1990).  
 [19] S. E. Rowley, C. Enderlein, J. F. de Oliveira, D. A. Tompsett, E. B. Saitovitch, S. S. Saxena, and G. G. Lonzarich, *arXiv:1801.08121*.  
 [20] J. R. Arce-Gamboa and G. G. Guzmán-Verri, *arXiv:1801.08736*.  
 [21] M. Cyrot, *Rep. Prog. Phys.* **36**, 103 (1973).  
 [22] A. F. Devonshire, *The London, Edinburgh, and Dublin Philosophical Magazine and Journal of Science* **40**, 1040 (1949).  
 [23] G. Bruls, D. Weber, B. Wolf, P. Thalmeier, B. Lüthi, A. de Visser, and A. Menovsky, *Phys. Rev. Lett.* **65**, 2294 (1990).  
 [24] C. W. Hicks, D. O. Brodsky, E. A. Yelland, A. S. Gibbs, J. A. N. Bruin, M. E. Barber, S. D. Edkins, K. Nishimura, S. Yonezawa, Y. Maeno, and A. P. Mackenzie, *Science* **344**, 283 (2014).  
 [25] T. Arpornthip, A. V. Balatsky, M. J. Graf, and Z. Nussinov, *Phys. Rev. B* **84**, 174304 (2011).

- [26] J. A. Aronovitz, P. Goldbart, and G. Mozurkewich, *Phys. Rev. Lett.* **64**, 2799 (1990).
- [27] A. T. Dorsey, P. M. Goldbart, and J. Toner, *Phys. Rev. Lett.* **96**, 055301 (2006).
- [28] B. Lautrup, *Physics of Continuous Matter* (IOP Publishing, Bristol, 2005).
- [29] T. Suzuki, Y. Nishi, and M. Fujimoto, *Philos. Mag. A* **80**, 621 (2000).
- [30] M. Sigrist, R. Joynt, and T. M. Rice, *Phys. Rev. B* **36**, 5186 (1987).
- [31] H. Noad, E. M. Spanton, K. C. Nowack, H. Inoue, M. Kim, T. A. Merz, C. Bell, Y. Hikita, R. Xu, W. Liu, A. Vailionis, H. Y. Hwang, and K. A. Moler, *Phys. Rev. B* **94**, 174516 (2016).
- [32] A. Antons, J. B. Neaton, K. M. Rabe, and D. Vanderbilt, *Phys. Rev. B* **71**, 024102 (2005).
- [33] Y. L. Li, S. Choudhury, J. H. Haeni, M. D. Biegalski, A. Vasudevarao, A. Sharan, H. Z. Ma, J. Levy, V. Gopalan, S. Trolier-McKinstry, D. G. Schlom, Q. X. Jia, and L. Q. Chen, *Phys. Rev. B* **73**, 184112 (2006).
- [34] G. Sheng, Y. L. Li, J. X. Zhang, S. Choudhury, Q. X. Jia, V. Gopalan, D. G. Schlom, Z. K. Liu, and L. Q. Chen, *Appl. Phys. Lett.* **96**, 232902 (2010).
- [35] K. Ueno, S. Nakamura, H. Shimotani, H. Yuan, N. Kimura, T. Nojima, H. Aoki, Y. Iwasa, and M. Kawasaki, *Nat. Nanotechnol.* **6**, 408 (2011).
- [36] G. Kresse and J. Furthmüller, *Phys. Rev. B* **54**, 11169 (1996).
- [37] J. P. Perdew, A. Ruzsinszky, G. I. Csonka, O. A. Vydrov, G. E. Scuseria, L. A. Constantin, X. Zhou, and K. Burke, *Phys. Rev. Lett.* **100**, 136406 (2008).
- [38] A. Togo and I. Tanaka, *Scr. Mater.* **108**, 1 (2015).
- [39] R. C. Powell, *Symmetry, Group Theory, and the Physical Properties of Crystals* (Springer, New York, 2010).
- [40] A. Okazaki and M. Kawaminami, *Mater. Res. Bull.* **8**, 545 (1973).
- [41] F. W. Lytle, *J. Appl. Phys.* **35**, 2212 (1964).
- [42] L. Rimai and G. A. deMars, *Phys. Rev.* **127**, 702 (1962).
- [43] P. A. Fleury, J. F. Scott, and J. M. Worlock, *Phys. Rev. Lett.* **21**, 16 (1968).
- [44] R. O. Bell and G. Rupprecht, *Phys. Rev.* **129**, 90 (1963).
- [45] G. Rupprecht and W. H. Winter, *Phys. Rev.* **155**, 1019 (1967).
- [46] C. W. Bark, D. A. Felker, Y. Wang, Y. Zhang, H. W. Jang, C. M. Folkman, J. W. Park, S. H. Baek, H. Zhou, D. D. Fong, X. Q. Pan, E. Y. Tsymbal, M. S. Rzchowski, and C. B. Eom, *Proc. Natl. Acad. Sci. U.S.A.* **108**, 4720 (2011).